The Astronomical Journal, 139:329–341, 2010 February doi:10.1088/0004-6256/139/2/329

THE CLUSTER AGES EXPERIMENT (CASE). IV. ANALYSIS OF THE ECLIPSING BINARY V69 IN THE GLOBULAR CLUSTER 47 Tuc*

I. B. Thompson[1], J. Kaluzny[2], S. M. Rucinski[3], W. Krzeminski[4], W. Pych[2], A. Dotter[5], and G. S. Burley[1]
[1] Carnegie Observatories, 813 Santa Barbara Street, Pasadena, CA 91101-1292, USA; ian@obs.carnegiescience.edu, burley@obs.carnegiescience.edu
[2] Copernicus Astronomical Center, Bartycka 18, 00-716 Warsaw, Poland; jka@camk.edu.pl, pych@camk.edu.pl
[3] David Dunlap Observatory, Department of Astronomy and Astrophysics, University of Toronto, P.O. Box 360, Richmond Hill, ON L4C 4Y6, Canada; rucinski@astro.utoronto.ca
[4] Las Campanas Observatory, Casilla 601, La Serena, Chile; wojtek@lco.cl
[5] Department of Physics and Astronomy, University of Victoria, P.O. Box 3055, Victoria, B.C. V8W 3P6, Canada; dotter@uvic.ca
Received 2008 October 6; accepted 2009 November 2; published 2009 December 16

ABSTRACT

We use photometric and spectroscopic observations of the eclipsing binary V69-47 Tuc to derive the masses, radii, and luminosities of the component stars. Based on measured systemic velocity, distance, and proper motion, the system is a member of the globular cluster 47 Tuc. The system has an orbital period of 29.5*d* and the orbit is slightly eccentric with $e = 0.056$. We obtain $M_p = 0.8762 \pm 0.0048\, M_\odot$, $R_p = 1.3148 \pm 0.0051\, R_\odot$, $L_p = 1.94 \pm 0.21\, L_\odot$ for the primary and $M_s = 0.8588 \pm 0.0060\, M_\odot$, $R_s = 1.1616 \pm 0.0062\, R_\odot$, $L_s = 1.53 \pm 0.17\, L_\odot$ for the secondary. These components of V69 are the first Population II stars with masses and radii derived directly and with an accuracy of better than 1%. We measure an apparent distance modulus of $(m - M)_V = 13.35 \pm 0.08$ to V69. We compare the absolute parameters of V69 with five sets of stellar evolution models and estimate the age of V69 using mass–luminosity–age, mass–radius–age, and turnoff mass–age relations. The masses, radii, and luminosities of the component stars are determined well enough that the measurement of ages is dominated by systematic differences between the evolutionary models, in particular, the adopted helium abundance. By comparing the observations to Dartmouth model isochrones we estimate the age of V69 to be 11.25 ± 0.21(random) $\pm$ 0.85(systematic) Gyr assuming [Fe/H] $= -0.70$, $[\alpha/\mathrm{Fe}] = 0.4$, and $Y = 0.255$. The determination of the distance to V69, and hence to 47 Tuc, can be further improved when infrared eclipse photometry is obtained for the variable.

Key words: binaries: close – binaries: spectroscopic – globular clusters: individual (47 Tuc) – stars: individual (V69 47 Tuc)

1. INTRODUCTION

Detached eclipsing double-line binary (DEB) stars are the fundamental astrophysical laboratory for the determination of stellar parameters of mass and radius. Luminosities can be derived using measured parallaxes or from empirical color–effective temperature relations. These data are the fundamental tests of stellar evolution models. Many field Population I systems are known at solar mass and larger (Andersen 1991) and modern high accuracy measurements of masses, luminosities, and radii of the component stars are in general agreement with evolution models (see, for example, Lacy et al. 2005, 2008; Clausen et al. 2008). Similar results are obtained for studies of individual binaries in the old open clusters NGC 188 (Meibom et al. 2009), NGC 2243 (Kaluzny et al. 2006), and NGC 6791 (Grundahl et al. 2008). Recent wide-field photometric surveys have identified numerous low-mass systems, and for these K and M stars the common theme of a comparison of component properties with evolution models is that the models systematically underestimate the radii of the components in these binaries. Summaries of recent measurements can be found in López-Morales et al. (2006), López-Morales (2007), and Blake et al. (2008).

The situation is even less clear for Population II stars. With the exception of CM Dra, for which the component masses are $\sim 0.2\, M_\odot$ (Lacy 1977), and the ω Cen binary OGLEGC-V17, for which the analysis is compromised by an uncertain determination of the metallicity (Thompson et al. 2001; Kaluzny et al. 2002), there are no known Population II DEBs with main-sequence components. Torres et al. (2002) used interferometric observations of HD 195987 ([Fe/H] ~ -0.6) to derive an orbit and measure the masses of the components. The radiative properties of the two components agree with a suite of models given some slight modifications of input parameters. While direct measurements of the radii of the components are not possible because HD 195987 is not an eclipsing binary, estimates of the radii can be derived from the orbital parallax, the bolometric flux, and the estimated effective temperatures. Here again the measured radii are larger than the models by some 10%. Boyajian et al. (2008) have measured the angular diameter of the G subdwarf μ Cas ([Fe/H ~ -0.8). This measurement provides a radius when combined with the Hipparcos parallax for μ Cas. For this star the models underpredict this measured radius by about 5%. The masses of the components of μ Cas are only known to about 10%, so the model comparisons here are not well constrained.

There is a clear need to locate and study Population II detached eclipsing binary stars to obtain accurate masses and radii of their component stars. Stellar evolution models are becoming increasingly sophisticated and are used to fit observed cluster color–magnitude diagrams (CMD). The cluster CMD's are themselves improving in quality, with homogeneous surveys being conducted with the *Hubble Space Telescope* (*HST*; see, for example, Sarajdeni et al. 2007). Careful empirical tests of these models are an essential next step.

This is the first paper in a series devoted to the study of DEBs in Galactic globular clusters with components on the cluster main sequence or subgiant branch. The Cluster

* This paper includes data gathered with the 6.5 m Magellan Baade and Clay Telescopes and the 2.5 m du Pont Telescope located at Las Campanas Observatory, Chile. It is based in part on data obtained at the South African Astronomical Observatory.

AgeS Experiment (CASE) has the goal of determining the basic stellar parameters (masses, luminosities, and radii) of the components of cluster binaries to a precision of better than 1% in order to measure cluster ages and distances, and to test stellar evolution models. The methods and assumptions utilize basic and simple approaches offered by the field of eclipsing double-line spectroscopic binaries as described in Paczyński (1997) and Thompson et al. (2001). Previous CASE papers have discussed blue straggler systems in ω Cen (Kaluzny et al. 2007a) and 47 Tuc (Kaluzny et al. 2007b), and an SB1 binary in NGC 6397 (Kaluzny et al. 2008).

The eclipsing binary V69-47 Tuc (hereinafter V69) was discovered by Weldrake et al. (2004) during a survey for variable stars in the field of the globular cluster 47 Tuc. They presented an *I*-band light curve for the variable and proposed an orbital period of $P = 5.229$ d. The light curve phased with this period shows only one eclipse. The variable is located at the top of main sequence in the cluster color–magnitude diagram, and thus is of potential great interest for measurements of the cluster age and distance.

In this paper, we report the results of photometric and spectroscopic observations aimed at a determination of the absolute parameters of the components of V69. Section 2 describes the photometry of the variable and the determination of an orbital ephemeris. Section 3 presents the radial velocity observations. The combined photometric and spectroscopic element solutions are given in Section 4 while the membership in 47 Tuc is discussed in Section 5. In Section 6, we compare the properties of the components of V69 to a selection of stellar evolution models with an emphasis on estimating the age of the system. Finally, in Section 7 we summarize our findings.

2. PHOTOMETRIC OBSERVATIONS

The bulk of the photometric data were obtained with the 1.0 m Swope telescope at the Las Campanas Observatory using the 2048 × 3150 pixel SITe3 CCD camera with a scale of 0.435 arcsec pixel^{-1}. These observations were collected during the 2004–2007 observing seasons. The same set of *BV* filters was used for all observations. Exposure times ranged from 100 s to 360 s for the *V* filter (average exposure was 120 s) and from 160 s to 360 s for the *B* filter (average exposure was 170 s). An eclipse event was detected on the first of a total of eight nights of observations during the 2004 season. When the 2004 season data were combined with the observations of Weldrake et al. (2004) we were able to eliminate the proposed 5.25 d period, but the combined data set was insufficient to establish a unique ephemeris. We then examined the 286 *V* band images collected by the OGLE team on 44 nights during the 1993 observing season for the cluster field 104-A (Kaluzny et al. 1998). A single eclipse event was detected on the night of 1993 July 22 UT and this permitted the identification of an approximate orbital period of $P \approx 29.540$ d. Subsequent observations collected in the 2005, 2006, and 2007 seasons concentrated on nights with predicted eclipse events. During the 2007 season we observed the variable with the 2.5 m du Pont telescope using the 2048 × 2048 pixel TEK5 CCD camera at a scale of 0.″259 pixel^{-1}. These data included one well covered primary eclipse observed mostly in the *V* band on 2007 August 18 UT.

In addition to the Las Campanas photometry, we obtained *V*-band observations of an eclipse on 2005 October 22 UT using the 1.0 m telescope at the South African Astronomical Observatory. Observations were obtained with the STE4 1024 × 1024 pixel CCD camera at a scale of 0.″31 pixel^{-1}.

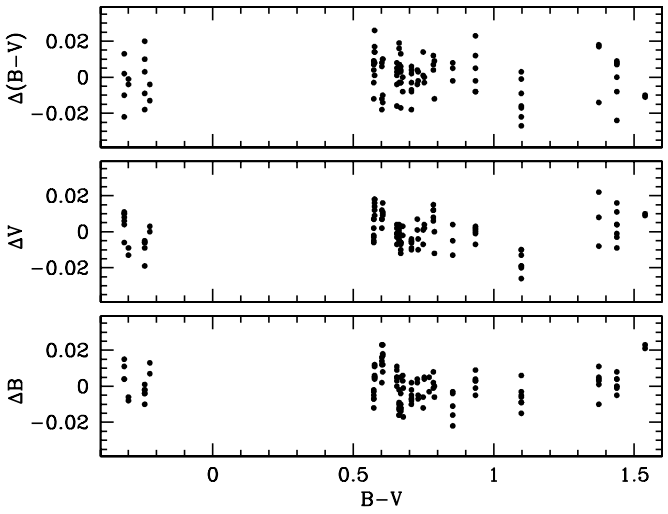

Figure 1. Plot of the color and magnitude residuals for the standard stars observed on the night of 2007 August 19.

Profile photometry was extracted for all of the observations using the DAOPHOT/ALLSTAR package (Stetson 1987). We calibrated the instrumental photometry using observations collected with the du Pont telescope on the night of 2007 August 19 UT. Observations were made of V69 together with four Landolt standard fields (Landolt 1992). The standards were observed with a range of air mass of $1.19 < X < 1.94$. The conditions were photometric and the seeing ranged from 1.05 to 1.40 arcsec with a median value of 1.22 arcsec. The images of the cluster itself were obtained at an air mass of 1.38 with seeing of 1.0 arcsec. Profile photometry for the field of the variable was extracted from subframes covering 220 × 180 arcsec (the full field of TEK5 camera is 8.65 × 8.65 arcmin). This helped to minimize the effects of a variable point-spread function and as a result to obtain reliable aperture corrections. Aperture corrections for the V69 observations and the standard field observations were derived using the program DAOGROW (Stetson 1990). Magnitudes of 28 standard stars in the Landolt fields were taken from the Stetson catalog (Stetson 2000).[6] The following relations between instrumental (lower case letters) and standard magnitudes were obtained:

$$v = V - 0.026(2) \times (B - V) + 0.118(3) \times X + \text{const}, \quad (1)$$

$$b = B - 0.069(2) \times (B - V) + 0.217(3) \times X + \text{const}, \quad (2)$$

where *X* is the air mass. In Figure 1, we show the residuals between the standard and recovered magnitudes for the Landolt primary standards. The analyzed V69 field includes 20 additional secondary standard stars from the Stetson catalog (Stetson 2000). The average residuals for these stars are $\Delta V = +0.004 \pm 0.019$ and $\Delta(B - V) = -0.001 \pm 0.015$ with our magnitudes fainter and our colors bluer on average.

A total of eight primary and six secondary eclipses were observed in the combined data sets. In Figure 2, we show the *BV* light curves of V69 phased with the ephemeris:

$$\text{Min } I = \text{HJD}2453237.8421(2) + 29.53975(1). \quad (3)$$

[6] We have used the electronic version of the catalog as of 2007 November 7. The catalog is maintained by Canadian Astronomy Data Centre at http://www3.cadc-ccda.hia-iha.nrc-cnrc.gc.ca/community/STETSON/standards/

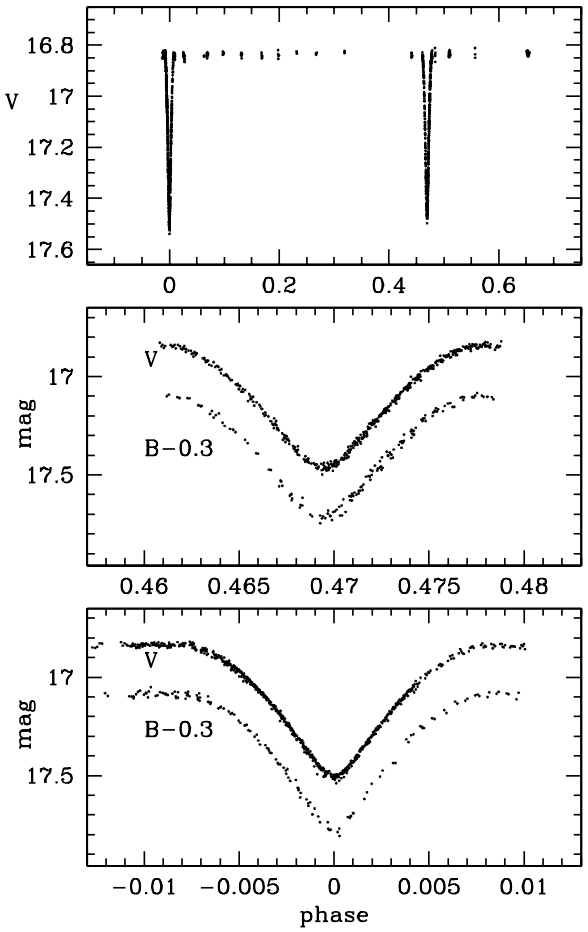

Figure 2. Phased BV light curves of V69.

Table 1
BV Photometry of V69 at Minima and Quadrature

Phase	V	B	$B-V$
Max	16.836(1)	17.384(2)	0.548(2)
Min I	17.507(3)	18.083(12)	0.576(12)
Min II	17.461(3)	18.011(14)	0.550(14)

The period was derived using the Lafler–Kinman algorithm, and the error in the period was estimated by visual inspection of the phased light curve as the period was varied away from the best fit value. These light curves contain a total of 1216 and 310 data points for V and B, respectively. The plots include photometry from all four data sets mentioned above. For the OGLE data we have plotted only points inside the primary eclipse. The colors and magnitudes of V69 at minima and at quadrature are listed in Table 1. The quoted errors do not include possible systematic errors of the zero points of the photometric solution which we estimate to be 0.010 mag.

3. SPECTROSCOPIC OBSERVATIONS

We obtained spectroscopic observations of V69 with the MIKE echelle spectrograph (Bernstein et al. 2003) on the Magellan Clay 6.5 m telescope. All observations were taken with a 0.7 arcsec slit at a resolution of $R \simeq 40{,}000$. The observations generally consisted of two exposures flanking an exposure of a thorium–argon hollow-cathode lamp. Total exposure times per spectrum ranged from 1300 to 3665 s depending on observing conditions. The observations were reduced with pipeline software written by Dan Kelson following the approach of Kelson (2003). Post-extraction processing of the spectra was done within the IRAF ECHELLE package.[7]

Table 2
Radial Velocity Observations of V69

HJD (−2400000)	V_p (km s^{-1})	V_s (km s^{-1})	Phase
53183.88089	−57.33	24.10	0.173
53201.93116	21.23	−55.92	0.784
53206.81454	−5.58	−28.40	0.950
53206.93425	−7.00	−27.15	0.954
53210.82680	−41.09	8.46	0.085
53210.93896	−42.27	9.98	0.089
53271.78367	−53.96	20.75	0.149
53274.77303	−59.04	26.63	0.250
53280.65021	−23.44	−9.68	0.449
53281.65012	−14.50	−18.34	0.483
53282.69872	−7.02	−26.32	0.519
53521.93280	12.54	−45.81	0.617
53580.91364	11.43	−46.41	0.614
53581.85305	16.04	−50.05	0.646
53582.85552	19.69	−53.69	0.680
53584.80006	22.23	−56.51	0.745
53585.79822	21.34	−55.77	0.779
53631.71181	−50.28	16.17	0.334
53633.74856	−36.21	1.48	0.402
53634.76492	−27.12	−6.54	0.437
53889.93336	−37.97	6.09	0.075
53891.93240	−52.13	20.77	0.143
53892.93208	−56.74	24.68	0.177
53893.93261	−59.42	26.95	0.210
53935.93349	14.75	−48.09	0.632
53937.92995	21.18	−55.15	0.700
53938.92894	22.39	−56.40	0.734

Velocities were measured with the TODCOR algorithm (Zucker & Mazeh 1994) using an implementation written by G. Torres. For velocity templates we used synthetic echelle resolution spectra from the grid of Coelho et al. (2006). We adopted the values of log g and $T_{\rm eff}$ derived from the photometric solution (see Section 4) and assumed a metallicity of [Fe/H] $= -0.71$ with an α-element enhancement of 0.4 (see the discussion of the metallicity of 47 Tuc in Section 4). The templates were adjusted once during the iterations for the Wilson–Devinney solutions, and final linear interpolations on the Coelho et al. grid were made at (log g, $T_{\rm eff}$, and [Fe/H]) = (4.14, 5945 K, −0.71) for the primary and (4.24, 5955 K, −0.71) for the secondary. The measured velocities are insensitive to minor changes in these parameters. The interpolated synthetic spectra were smoothed with a Gaussian to match the resolution of the observations. No rotational broadening was applied to the templates. The cross-correlations covered the wavelength intervals 4125 Å $< \lambda <$ 4320 Å, 4350 Å $< \lambda <$ 4600 Å, and 4600 Å $< \lambda <$ 4850 Å. The final adopted velocities are the averages of these three measurements for each of the observations.

The measured radial velocities were fit with a non-linear least-squares solution using code written by G. Torres adopting the ephemeris given in Equation (3). The observations are presented in Table 2 which lists the Heliocentric Julian Date (HJD) at mid-exposure, the velocities of the primary and secondary

[7] IRAF is distributed by the National Optical Astronomy Observatories, which are operated by the Association of Universities for Research in Astronomy, Inc., under cooperative agreement with the NSF.

Table 3
Orbital Parameters for V69

Parameter	Value
P (days)	29.53975[a]
T_0 (HJD−2400000)	2453237.8421[a]
γ (km s^{-1})	−16.71 ± 0.05
K_p (km s^{-1})	41.03 ± 0.13
K_s (km s^{-1})	41.86 ± 0.09
e	0.0563 ± 0.0011
ω (deg)	149.15 ± 1.86
σ_p (km s^{-1})	0.50
σ_s (km s^{-1})	0.33
Derived quantities	
$A \sin i$ ($R_\odot$)	48.301 ± 0.095
$M_p \sin^3 i$ ($M_\odot$)	0.8762 ± 0.0048
$M_s \sin^3 i$ ($M_\odot$)	0.8588 ± 0.0060

Notes. [a] Ephemeris adopted from photometry.

components, and the orbital phases of the observations. The adopted orbital elements are listed in Table 3 and the orbit is plotted in Figure 3.

4. LIGHT CURVE ANALYSIS AND SYSTEM PARAMETERS

We have used two different models for the analysis of the light curves. The first is the Wilson–Devinney model (Wilson & Devinney 1971; Wilson 1979) as implemented in the PHOEBE package (Prša & Zwitter 2005). The second is the JKTEBOP program (Southworth et al. 2004a, 2004b), which is based on the EBOP code (Popper 1980; Popper & Etzel 1981; Etzel 1981). The most recent public version of JKTEBOP is described in detail in Southworth et al. (2007). In particular, it incorporates an option to adopt a non-linear limb darkening law.

The two light-curve fitting programs utilize different methodologies and approaches. The PHOEBE/WD program is more sophisticated in its treatment of the geometry and the stellar atmospheres. It utilizes the Roche geometry to approximate the shapes of the stars, uses the Kurucz model atmospheres, and treats the reflection effect in detail. It can be used for any component separation including contact systems. JKTEBOP/EBOP approximates stars by bi-axial ellipsoids. It is faster than the WD code but is appropriate only for binary components that are spherical or only slightly distorted. The real advantage of JKTEBOP is that the errors for the fit parameters are reliably determined. The PHOEBE code provides only formal errors of the fits and these are known to be underestimated (A. Prsa 2006, private communication). However, an advantage of the PHOEBE code is that it can be used for the analysis of multi-color light curves. For V69 the solution for the B band is much poorer than for the V band because of the lower quality of the B band data. PHOEBE/WD was used to simultaneously fit the V and B curves. The resulting geometrical parameters are based mostly on the higher quality V curve while the simultaneous fit permits a good estimate of the luminosity ratio.

In the analysis, we assumed that the light curve of V69 is free from any "third light." This is supported by the depths of the eclipses, with $\Delta V > 0.63$ mag for both the primary and secondary eclipse. There is also no evidence for any third component in the spectra of the binary. Finally, we note that V69 can be located on numerous *HST*/ACS images (for example, PEP ID 9018, P.I. G. De Marchi). Examination of these images indicates that our ground-based photometry does not suffer from any blending problems from unresolved visual companions to the variable.

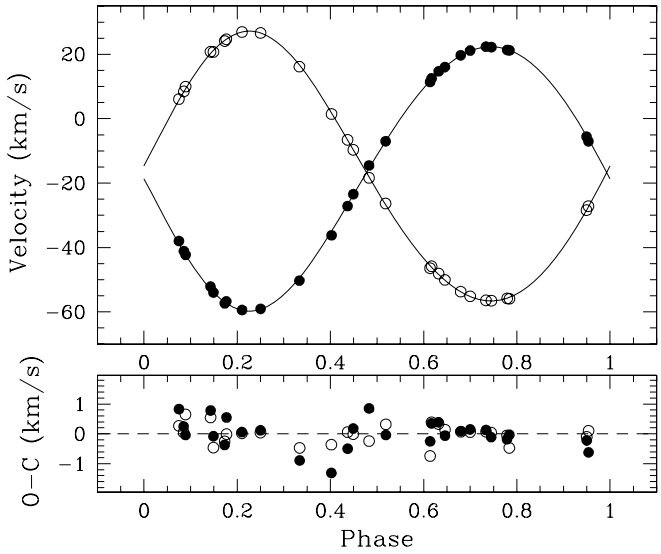

Figure 3. Radial velocity observations of V69. Filled symbols represent data for the primary and open symbols are for the secondary.

Four recent high-resolution studies of the metallicity of 47 Tuc suggest a value of [Fe/H] ∼ −0.7. As part of a study to establish a globular cluster metallicity scale based on measurements of Fe II lines, Kraft & Ivans (2003) reanalyzed in a uniform way equivalent widths in a total of eight giants measured by Brown & Wallerstein (1992), Norris & Da Costa (1995), and Carretta & Gratton (1997). They obtained a range of −0.61 to −0.69 for $[Fe/H]_I$ and a range of −0.56 to −0.70 for $[Fe/H]_{II}$. Alves-Brito et al. (2005) used observations of five giants to obtain $[Fe/H]_I = -0.66$ and $[Fe/H]_{II} = -0.69$ with an α-element enhancement of about 0.3 dex. Koch & McWilliam (2008) found $[Fe/H]_I = -0.76$ and $[Fe/H]_{II} = -0.82$ with an α-element enhancement of 0.4 dex based on a study of eight giants and one dwarf star. Finally, Carretta et al. (2009) measured $[Fe/H]_I = -0.77$ and $[Fe/H]_{II} = -0.80$ with an α-element enhancement of +0.39 from observations of 11 giants. For this analysis, we have adopted a value of [Fe/H] = −0.71 together with an α-element enhancement of +0.4. Sensitivities of age estimates to these assumptions are explored in Sections 6.1 and 6.2.

The effective temperature of the primary is needed for the PHOEBE light-curve solution and for both components to estimate the luminosities of the stars from the derived radii. In the absence of detailed infrared eclipse photometry we estimated the effective temperature of the primary, T_p, from the dereddened $(B - V)$ and $(V - I)$ color indices. We used the observed color of the binary, $(B - V) = 0.548$ (see Table 1) together with a reddening of $E(B-V) = 0.04$ (Harris 1996; Gratton et al. 2003; Percival et al. 2002) to derive $(B-V)_0 = 0.508$. For the $(V - I)$ color we note that V69 is star number 14065 in the catalog of Kaluzny et al. (1998) where $(V - I) = 0.731 \pm 0.025$. We shift this observed color by −0.026 to put the observation on the system of Stetson (2000) (Percival et al. 2002) and adopt the reddening law of Schlegel et al. (1998) to obtain $E(V - I) = 0.06$ and a final value of $(V - I)_0 = 0.671$. The similarity of the $(B - V)$ colors in and out of eclipse (see Table 1) suggests that the effective temperature of the primary derived from these colors is close to the true value.

Visual inspection of the position of the binary in a color–magnitude diagram suggests that the components are beginning

Table 4
Results of the Light Curve Analysis for V69 Obtained with the PHOEBE Code

Parameter	Value
i (deg)	89.771 ± 0.009
T_p (K)	5945
T_s (K)	5959 ± 3
e	0.0556 ± 0.0002
ω (deg)	149.72 ± 0.25
r_p	0.02727 ± 0.00005
r_s	0.02408 ± 0.00008
$(L_s/L_p)_V$	0.7870 ± 0.0012
$(L_s/L_p)_B$	0.7889 ± 0.0015
$\sigma_{\rm rms}(V)$ (mmag)	10.0
$\sigma_{\rm rms}(B)$ (mmag)	14.5

to evolve away from the main sequence (see Figure 4), and so we adopt an initial gravity for the primary of $\log g = 4.1$.

These adopted colors and parameters lead to estimates for the effective temperature of the primary of 6070 K and 5900 K, 6050 K and 5905 K, and 5960 K and 5780 K for the $(B - V)$ and $(V - I)$ colors and the calibrations of Worthey & Lee (2006), Ramirez & Meléndez (2005), and VandenBerg & Clem (2003), respectively. We adopt a linear average of these estimates, resulting in an effective temperature for the primary of 5945±105 K, where the quoted error is the standard deviation of the six temperature estimates.

The three color–temperature relations considered here do not explicitly account for α-element enhancement. Based on the synthetic color–temperature employed by Dotter et al. (2007), we estimate that the difference in $T_{\rm eff}$ between $[\alpha/{\rm Fe}] = 0$ and +0.4 is ∼10 K for the [Fe/H], $T_{\rm eff}$, and $\log g$ of the primary. We expect this is an upper limit because the color–temperature relations should include some implicit dependence on $[\alpha/{\rm Fe}]$. In any case, the $[\alpha/{\rm Fe}]$-color uncertainty is small compared to that which arises between the different color–temperature relations or between $B - V$ and $V - I$.

We note that Koch & McWilliam (2008) adopted an effective temperature of 5750 K for the turnoff star that they studied based on excitation equilibrium for Fe I lines, and it is of interest to ask how accurate our photometric estimate of the effective temperature of the primary of V69 actually is. We estimate the uncertainty in the reddening to be 0.010 mag, and this value coupled with our estimated uncertainty in the photometric calibration suggests that the uncertainty in the derived unreddened $(B - V)$ colors of the components of V69 to be ∼0.014 mag. The $(V - I)$ color is somewhat less accurate. For a range of metallicity of [Fe/H] from −0.61 to −0.77 (see above), an estimated range in the gravity of 0.2 dex and a uncertainty in $(B - V)_0$ of 0.014, the Worthey–Lee calibration suggests an uncertainty in the derived effective temperature of approximately 80 K. The calibrations of Ramirez & Meléndez (2005) and VandenBerg & Clem (2003) indicate similar uncertainties. Considering the scatter about $T_{\rm eff}$ in the various calibrations we conservatively conclude that we can estimate the effective temperature of the components of V69 to an accuracy of about 150 K. These three calibrations predict bolometric corrections spanning the range −0.11 to −0.09 and we adopt ${\rm BC}_p = {\rm BC}_s = -0.10 \pm 0.01$.

4.1. Models Using the PHOEBE Code

The PHOEBE implementation of the Wilson–Devinney model fits the orbital inclination i, the gravitational potentials Ω_p and Ω_s, the effective temperature of the secondary T_s, the eccentricity e, the longitude of the periastron ω, and the relative luminosities L_s/L_p in B and V simultaneously. We iterated on the solution, calculating subsequent values for the $(B-V)_0$ colors for the primary and secondary from the observed $(B-V)_0$ for the system and the modeled values for $(L_s/L_p)_B$ and $(L_s/L_p)_V$ at each iteration. The mass ratio was set to the spectroscopic value of $q = {\rm mass}_s/{\rm mass}_p = 0.984$. The iterations converged in two cycles. The final values of the fit are listed in Table 4. The values for the relative radii are derived directly from the nondimensional potentials Ω_1 and Ω_2, and the spectroscopic mass ratio q. The luminosity ratios and the relative radii are insensitive to changes in effective temperature: $(L_s/L_p)_B$, $(L_s/L_p)_V$, r_s, and r_p all change by less than 0.3% for a ±150 K change in effective temperature.

Table 5
Results of the Light Curve Analysis for V69 Obtained with the JKTEBOP Code

Parameter	V	B
Adjusted quantities		
$r_p + r_s$	0.05166 ± 0.00009	0.05151 ± 0.00021
$k = r_p/r_s$	0.8836 ± 0.0072	0.8961 ± 0.0199
i (deg)	89.768 ± 0.012	89.769 ± 0.028
J	1.0146 ± 0.0031	1.0022 ± 0.0091
e	0.0567 ± 0.0008	0.0586 ± 0.0025
ω (deg)	147.7 ± 1.3	145.2 ± 3.4
Other quantities		
r_p	0.02722 ± 0.00009	0.02717 ± 0.00026
r_s	0.02405 ± 0.00012	0.02435 ± 0.00033
L_s/L_p	0.792 ± 0.011	0.802 ± 0.028
$\sigma_{\rm rms}$ (mmag)	10.0	14.5

4.2. Models Using the JKTEBOP Code

The JKTEBOP code optimizes the sum of the relative radii $r_p + r_s$, the ratio $k = r_s/r_p$, the ratio of the surface brightness of the two stars J, the orbital eccentricity e, and the longitude of the periastron ω. These two last parameters were included in the analysis by fitting $e\cos\omega$ and $e\sin\omega$. The mass ratio was fixed at the spectroscopic value of $q = 0.984$, and the gravity brightening exponent was set to 0.32. Note that the values for these two parameters have a negligible effect on the model light curve as the stars are very well separated and both are practically spherical. We adopted a square-root law for the limb darkening and adopted theoretical limb darkening coefficients from van Hamme (1993) for $T_{\rm eff} = 5959$ K (adopted from the PHOEBE code solution) and [Fe/H] = −0.71.

Table 5 contains the values of the fit parameters along with other relevant parameters derived from the solution. The last two rows list the reduced Chi-squared of the fit and the rms of the residuals. Separate solutions were derived for light curves in the V and B bands. The uncertainties of individual parameters were estimated using Monte Carlo simulations as described in Southworth et al. (2004b). Ten thousand simulations were run for each light curve. The solution based on the V light curve is much better constrained than the solution for the B band. The residuals of the fit obtained with the JKTEBOP are shown in Figure 5.

4.3. Adopted Stellar Parameters

A comparison of Tables 4 and 5 shows that the two light-curve synthesis codes give very similar results. There is also good agreement between the fitted values of e and ω and those

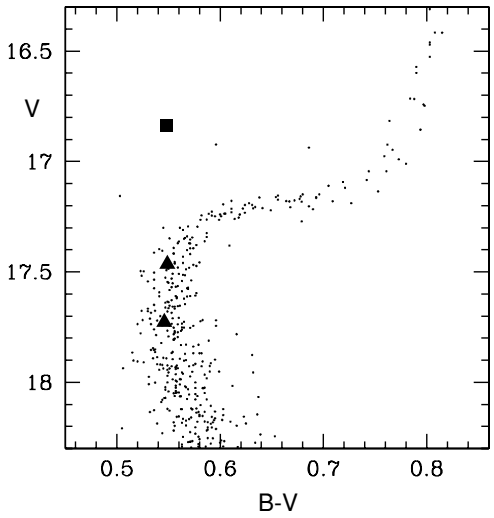

Figure 4. Position of V69 in the BV CMD for 47 Tuc. The square gives the position for the combined light and the triangles show the positions of each of the individual components.

derived from the spectroscopic observations. The remarkably small errors for the fit radii and relative luminosities might seem suspicious at first given that the light curves suggest that the eclipses of V69 are partial. However, the secondary eclipse is very close to being total. Examination of the synthetic light curves shows that only 0.4% of the surface of the secondary component remains visible at the center of the secondary eclipse.

The magnitudes for the individual components of the binary are derived from the luminosity ratios from the light-curve solution and the observed out-of-eclipse photometry. We obtain $V_p = 17.468 \pm 0.010$, $B_p = 18.019 \pm 0.010$, $V_s = 17.724 \pm 0.010$, and $B_s = 18.268 \pm 0.010$ where the errors are dominated by the contribution from zero point uncertainties of our photometry, estimated at 0.010 mag. The colors of both components are practically identical with $(B-V)_p = 0.551 \pm 0.014$ and $(B-V)_s = 0.544 \pm 0.014$. The position of the binary on the 47 Tuc color–magnitude diagram is shown in Figure 4. The primary component has left the main sequence of the cluster and is starting to ascend onto the subgiant branch. The secondary also has begun to evolve and is among the bluest stars at the cluster turnoff.

The absolute parameters of V69 obtained from our spectroscopic and photometric analysis are given in Table 6. Because the JKTEBOP code provides better error estimates than PHOEBE we have adopted the V band relative radii from Table 5. Note, however, that the relative radii derived with the PHOEBE models agree at a level of 0.2% with those obtained with the JKTEBOP models. The luminosities of the components follow directly from $\log(L/L_\odot) = 2\log(R/R_\odot) + 4\log(T_{\rm eff}/T_\odot)$ where we have adopted $R_\odot = 6.9598 \times 10^5$ km (Bahcall et al. 2005) and $T_\odot = 5777$ K (Neckel 1986).

5. MEMBERSHIP OF V69 AND THE DISTANCE OF 47 TUC

Before using the derived stellar parameters of the components of V69 to estimate the age of 47 Tuc, it is appropriate to consider the cluster membership of the star. There are four lines of evidence available. First, although the velocity of 47 Tuc is low at $v_{\rm rad} = -18.7 \pm 0.5$ km s^{-1} (Gebhardt et al. 1995), and thus does not provide a strong discriminant against projected field stars, the center-of-mass velocity of V69 ($\gamma = -16.36$ km s^{-1}) is consistent with this velocity. At the location of the variable—about 6 arcmin from the cluster center—the velocity dispersion of cluster stars is about 8 km s^{-1}. Second, Figure 4 shows that the individual components of V69 lie on the cluster main sequence. Third, the binary is a proper-motion member of 47 Tuc. The absolute proper motion of 47 Tuc has been measured to be $\mu_\alpha = 5.64 \pm 0.20$ mas yr^{-1} and $\mu_\delta = -2.05 \pm 0.20$ mas yr^{-1} (Anderson & King 2003). V69 is located in Field F of that study. This field has subsequently become a standard calibration field for *HST*, and V69 is present in numerous ACS/WFC frames taken between 2002 and 2006. A quick study of the ~30 s F606W exposures shows that the proper motion of V69 relative to the bulk of the cluster stars is 0.2 mas yr^{-1} in R.A. and −0.1 mas yr^{-1} in decl., a typical internal motion for a cluster member at this radius (J. Anderson 2008, private communication). Finally, based on the absolute magnitudes listed in Table 6 and the apparent magnitudes listed in Section 4.3 we derive distance moduli for the components of V69 of $(m-M)_V = 13.35 \pm 0.11$ and $(m-M)_V = 13.34 \pm 0.12$ for the primary and secondary, respectively. The average of these values is $(m-M)_V = 13.35 \pm 0.08$. We compare this value to some recent distance determinations for 47 Tuc in Table 7. While Bono et al. (2008) have shown that there appears to be some systematic errors in the measurement of the distance to 47 Tuc by different techniques, V69 clearly lies at the distance of 47 Tuc. We note in particular that Kaluzny et al. (2007b) find a distance modulus of $(m-M)_V = 13.40 \pm 0.08$ for OGLE-228, another eclipsing binary in 47 Tuc. We conclude that V69 is a member of the globular cluster 47 Tuc.

Table 6
Absolute Parameters for V69

Parameter	Value
A ($R_\odot$)	48.30 ± 0.12
M_p ($M_\odot$)	0.8762 ± 0.0048
M_s ($M_\odot$)	0.8588 ± 0.0060
R_p ($R_\odot$)	1.3148 ± 0.0051
R_s ($R_\odot$)	1.1616 ± 0.0062
T_p (K)	5945 ± 150
T_s (K)	5959 ± 150
$L_p^{\rm bol}$ ($L_\odot$)	1.94 ± 0.21
$L_s^{\rm bol}$ ($L_\odot$)	1.53 ± 0.17
$M_{\rm Vp}$ (mag)	4.12 ± 0.11
$M_{\rm Vs}$ (mag)	4.38 ± 0.12
$\log g_p$(cm s^{-2})	4.143 ± 0.003
$\log g_s$(cm s^{-2})	4.242 ± 0.003

6. THE AGE OF 47 TUC

The potential of using observations of eclipsing binaries for a robust determination of globular cluster ages was advocated by Paczyński (1997). In particular, he argued that the mass–luminosity–age relation be used rather than the mass–radius–age relation since the latter can be affected by inaccuracies in the stellar models related to the treatment of subphotospheric convection. In the following, we compare the properties of the components of V69 with five different sets of stellar evolution models. We have attempted to minimize the effects of metallicity and α-element enhancement by comparing models with uniform values of [Fe/H] = −0.71 and, where possible, [α/Fe] = +0.4.

In our analysis, we use the Dartmouth Stellar Evolution Database (Dotter et al. 2007), the Padova models (Salasnich

Table 7
Comparison of Distance Determinations to 47 Tuc

Author	Method	$(m-M)_V$
Gratton et al. (2003)	Main seq. fitting	13.50 ± 0.08
Percival et al. (2002)	Main seq. fitting	13.37 ± 0.11
Grundahl et al. (2002)	Main seq. fitting	13.33 ± 0.04 ± 0.1
Zoccali et al. (2001)	White dwarfs	13.27 ± 0.14
McLaughlin et al. (2006)	Kinematics	13.15 ± 0.13
Salaris et al. (2007)	IR luminosity of HB	13.18 ± 0.03 ± 0.04
Kaluzny et al. (2007b)	Eclipsing binary	13.40 ± 0.07
Bono et al. (2008)	Tip RG branch	13.32 ± 0.09
Bono et al. (2008)	IR luminosity of RR Lyrae stars	13.47 ± 0.11
This paper	Eclipsing binary	13.35 ± 0.08

Table 8
Parameters of Stellar Evolution Models

Parameter	Dartmouth	Padova	Teramo	Victoria	Yonsei–Yale
[Fe/H]	−0.71	−0.70	−0.70	−0.705	−0.71
[α/Fe]	+0.40	0.40	+0.40	+0.30	+0.40
X	0.738010	0.742000	0.736000	0.750250	0.748031
Y	0.255000	0.250000	0.256000	0.243000	0.244646
Z	0.006490	0.008000	0.008000	0.006750	0.007323
[O/Fe]	0.40	0.50	0.50	0.30	0.40
Mixing length	1.938	1.680	1.913	1.890	1.743
$(Z/X)_{solar}$	0.023	0.024	0.024	0.024	0.024

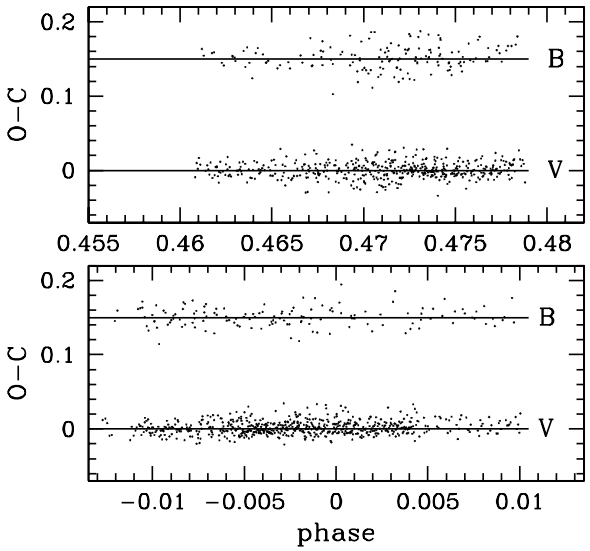

Figure 5. Residuals of the fits to the light curve obtained with JKTEBOP for the primary (bottom) and secondary eclipse (top). The residuals for *B* are offset by 0.15 mag for clarity.

et al. 2000), the Teramo models (Pietrinferni et al. 2006), the Victoria–Regina models (VandenBerg et al. 2006), and the Yonsei–Yale models (Kim et al. 2002).[8] Table 8 compares the parameters of each model set used in the derivation of the ages of V69. Entries for the solar abundance scale refer to Grevesse & Noels (1993) (Z/X ∼ 0.024)) and Grevesse & Sauval (1998) (Z/X ∼ 0.023). We note that solar models based on recent measurements of the solar abundance scale remain in conflict with helioseismology data (see Serenelli et al. (2009) for a discussion). We compare the derived values of mass, luminosity, and radius for the components of V69 with the isochrones. For the Dartmouth, Victoria–Regina, and Yonsei–Yale models we used interpolation software provided by the different groups to generate the plotted isochrones. For the Padova models we linearly interpolated on log (age) to generate isochrones spaced by 0.5 Gyr for ease of comparison with the other models.

We plot the components of V69 on the mass–luminosity and mass–radius planes for the Dartmouth, Padova, Teramo, Victoria–Regina, and Yonsei–Yale models in Figures 6, 7, 8, 9, and 10, respectively. In each figure, isochrones are shown with a step of 0.5 Gyr. The measured ages for the components of V69 are summarized in Table 9. To calculate the random errors in the age estimates we assumed that the measurement errors in mass, luminosity, and radius are uncorrelated. This is a reasonable assumption for the errors in luminosity are dominated by the adopted error in $T_{\rm eff}$ and the errors in radius are dominated by the photometric solution rather than the error in $A \sin i$ as measured by the orbital solution. The errors in mass, luminosity, and radius lead to uncertainties in age through comparison with the sets of isochrones, and the final random errors listed in Table 9 are the quadrature sums of the mass–radius and mass–luminosity age uncertainties. The uncertainties in the masses (about 0.6%) and in the luminosities (about 10%) give similar contributions to the errors of the derived ages, while the random errors in the age estimated from mass–radius–age relations are completely dominated by the measurement errors in the masses of the components. We emphasize that the plotted uncertainty in luminosity arises directly from the ±150 K uncertainty in the effective temperatures of the components of V69. The radii are measured with a better relative accuracy than the luminosities and therefore the ages can be derived with a random error a factor of 2 smaller than the ages derived from the mass–luminosity relations. Table 9 also presents the weighted average of the ages measured for the primary and secondary components of the binary.

[8] The models and supporting software are available at the following Web sites: Dartmouth (http://stellar.dartmouth.edu/∼models/), Padova (http://pleiadi.oapd.inaf.it/), Teramo (http://193.204.1.62/index.html), Victoria–Regina (http:www.cadc-ccda.hia-iha.nrccnrc.gc.ca/cvo/community/VictoriaReginaModels/), and Yonsei–Yale (http://www.astro.yale.edu/demarque/yyiso.html).

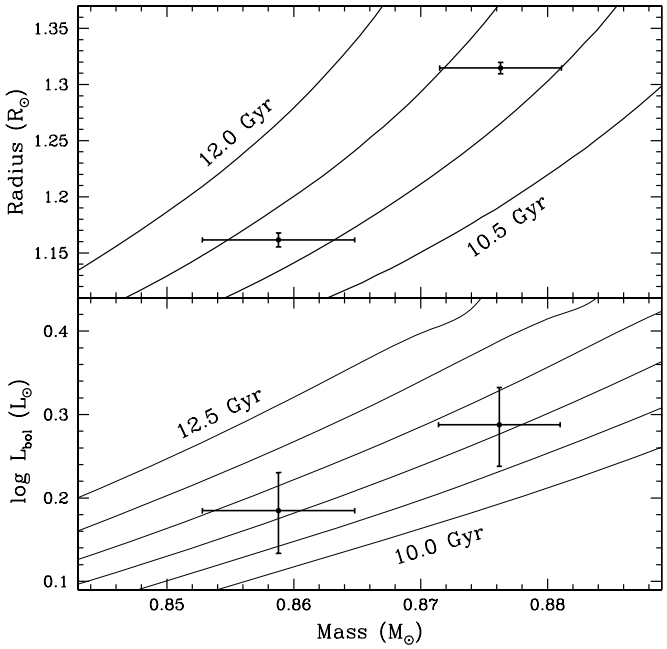

Figure 6. Masses, luminosities, and radii of the components of V69 are compared to isochrones based on the Dartmouth models. For each panel the isochrones are plotted in steps of 0.5 Gyr, with the lowest and highest age isochrones labeled.

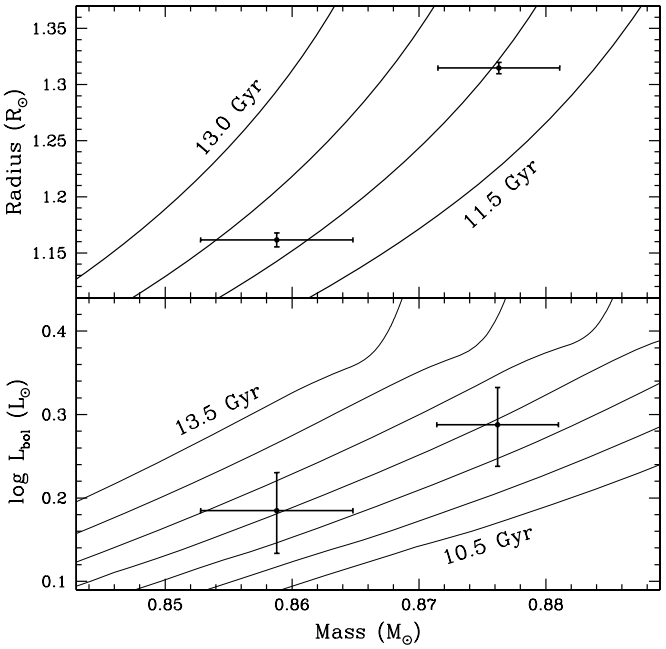

Figure 8. Masses, luminosities, and radii of the components of V69 are compared to isochrones based on the Teramo models. For each panel the isochrones are plotted in steps of 0.5 Gyr, with the lowest and highest age isochrones labeled.

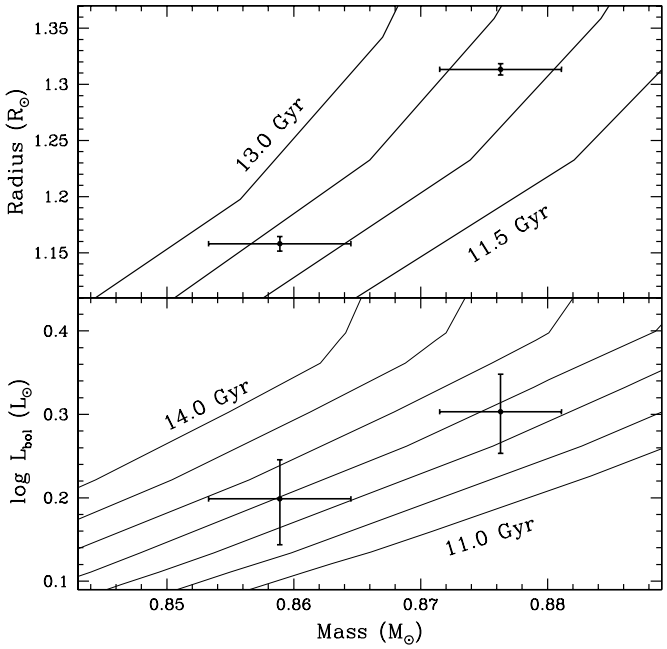

Figure 7. Masses, luminosities, and radii of the components of V69 are compared to isochrones based on the Padova models. For each panel the isochrones are plotted in steps of 0.5 Gyr, with the lowest and highest age isochrones labeled.

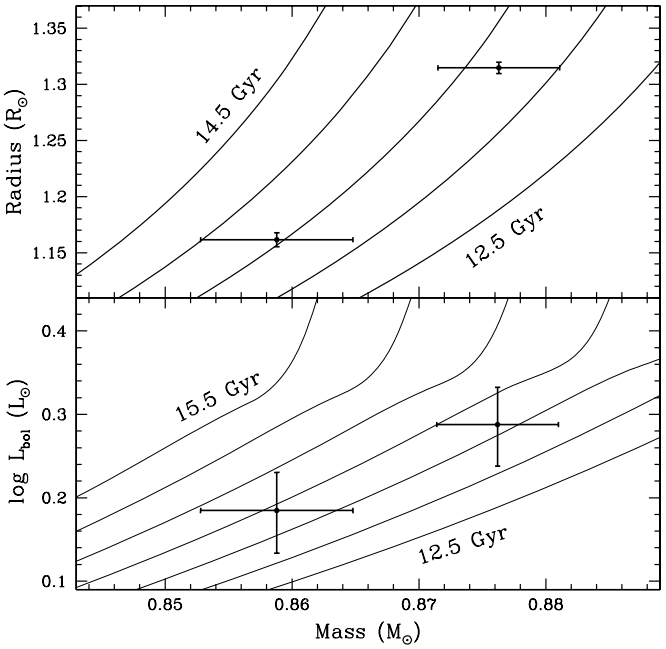

Figure 9. Masses, luminosities, and radii of the components of V69 are compared to isochrones based on the Victoria–Regina models. For each panel the isochrones are plotted in steps of 0.5 Gyr, with the lowest and highest age isochrones labeled.

Finally, since the components are very close to the cluster turnoff (see Figure 4), the age of the system can be estimated from turnoff mass–age relations. For each isochrone we estimated the turnoff mass as the mass at maximum $\log T_{\rm eff}$ in that isochrone. Based on the position of the components in the CMD we conclude that the secondary is at the blue extreme of the CMD, and that the primary has begun to evolve onto the subgiant branch at a slightly cooler effective temperature. Our mass measurements are accurate enough to resolve the progression of mass along an isochrone in this part of the CMD. Figure 11 shows the resulting relations, and these derived ages are also summarized in Table 9. For completeness, ages are also given for the primary assuming it is at the cluster turnoff. The quoted errors in these ages are derived assuming only an error in the measurement of the masses, and are measured from the values of the ages at the $\pm 1\sigma$ extrema of the measured masses. This age measurement is obviously fairly crude, but serves as a consistency check on the other ages estimates.

Table 9
Ages in Gyr for the Components of V69 Derived from Model Isochrones

Method	Component	Dartmouth	Padova	Teramo	Victoria–Regina	Yonsei–Yale
Mass–luminosity	Primary	11.11+0.54/−0.58	12.39+0.55/−0.62	11.93+0.55/−0.62	13.62+0.57/−0.66	13.02+0.54/−0.62
	Secondary	11.12+0.80/−0.93	12.46+0.80/−0.89	12.04+0.76/−0.93	13.90+0.68/−0.89	13.16+0.72/−0.81
	Average	11.11+0.45/−0.49	12.41+0.45/−0.51	11.97+0.45/−0.52	13.74+0.44/−0.53	13.07+0.43/−0.49
Mass–radius	Primary	11.25 ± 0.26	12.26 ± 0.29	11.97 ± 0.31	13.32 ± 0.33	12.63 ± 0.29
	Secondary	11.25 ± 0.37	12.34 ± 0.40	12.16 ± 0.42	13.54 ± 0.46	12.70 ± 0.39
	Average	11.25 ± 0.21	12.29 ± 0.24	12.04 ± 0.25	13.39 ± 0.27	12.65 ± 0.23
Turnoff mass	Primary	10.91 ± 0.24	11.81 ± 0.27	11.19 ± 0.25	12.50 ± 0.29	11.57 ± 0.26
	Secondary	11.75 ± 0.31	12.79 ± 0.37	12.15 ± 0.35	13.58 ± 0.40	12.52 ± 0.34

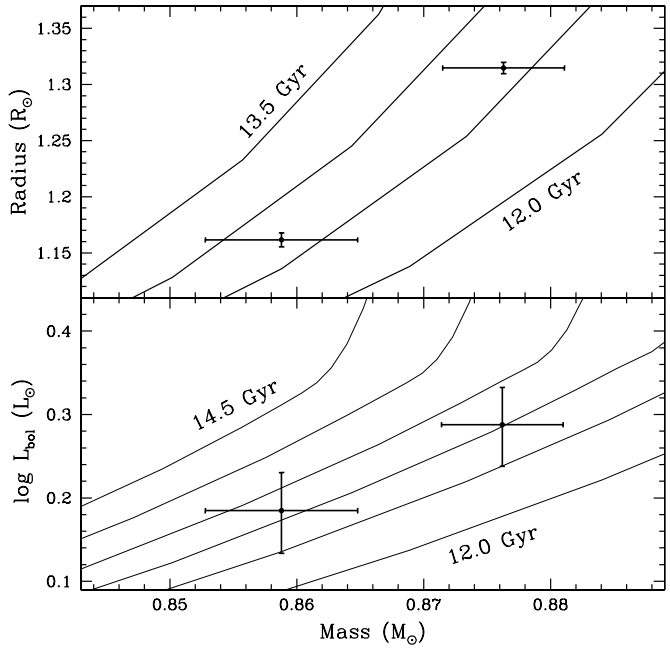

Figure 10. Masses, luminosities, and radii of the components of V69 are compared to isochrones based on the Yonsei–Yale models. For each panel the isochrones are plotted in steps of 0.5 Gyr, with the lowest and highest age isochrones labeled.

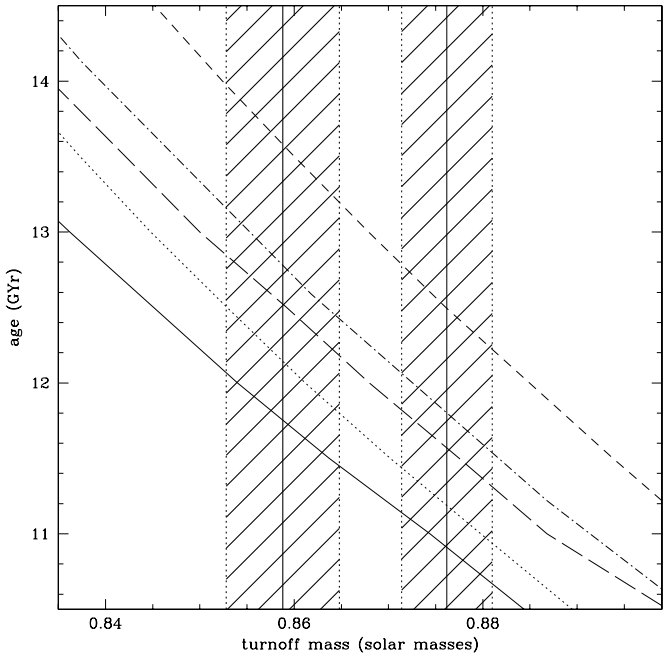

Figure 11. Age as a function of turnoff mass for the Dartmouth (solid line), Teramo (dotted line), Yonsei–Yale (long dashed line), Padova (dot-dashed line), and Victoria–Regina (short dashed line) models. The masses for the primary and secondary components of V69 are plotted as solid vertical lines, with one-sigma errors represented by the shaded areas about the component masses.

The ages of V69 determined from these relations show some considerable spread from one model set to the next, ranging from 11.1 to 13.7 Gyr. While we only have age estimates from two stars, we can draw some general conclusions. The first is that the close agreement in the age estimates for the primary and secondary for all models suggests that the errors in luminosity are overestimated. Second, the ages measured by the three methods also agree to within the random errors within each model. This suggests that concerns about the model radii arising from uncertainties in the treatment of convection are overstated, and that the models predict internally consistent luminosities and radii at the measured masses. Future studies of clusters with more binaries covering a wider range of mass will be important in addressing this second issue.

We next investigate whether or not there are systematic differences in the different model sets that might explain the wide range in measured ages. Many variables will affect the isochrones, among the most significant are adopted α-element enhancement and the relative abundance distribution over the α-elements, helium abundance, mixing length and convective overshoot, and the treatment of diffusion and gravitational settling. None of the models considered include the effects of rotation. Two of these variables ([Fe/H] and α-element enhancement) are measurable from spectroscopic data, while the others are parameters of the models.

In the following subsections, we explore the sensitivity of the measured ages to [Fe/H], [α/Fe], diffusion and gravitational settling, and helium abundance.

6.1. Sensitivity to Adopted [Fe/H]

Figure 12 shows the sensitivity of the measured ages to model [Fe/H] for the Dartmouth and Yonsei–Yale models sets for a range of ±0.05 dex around our adopted value of −0.71 for each of the three methods of measuring age. These values are interpolated in the models at a fixed [α/Fe] = +0.4. The plotted values are a weighted average of ages measured for the primary and secondary. The slopes (in terms of Δ Gyr per 0.1 dex) are given in Table 10. In all three cases the slopes for the two model sets are very similar, and Table 10 also gives the average slopes.

Table 10
Effect of [Fe/H] and [α/Fe] on Measured Age

Method	Model	[Fe/H] ΔGyr/0.1 dex	[α/Fe] ΔGyr/0.1 dex
Mass–luminosity	Dartmouth	1.09	0.67
	Yonsei–Yale	1.03	0.67
	Average	1.06	0.67
Mass–radius	Dartmouth	0.73	0.44
	Yonsei–Yale	0.79	0.54
	Average	0.76	0.49
Turnoff mass	Dartmouth	0.68	0.43
	Yonsei–Yale	0.78	0.37
	Average	0.73	0.40

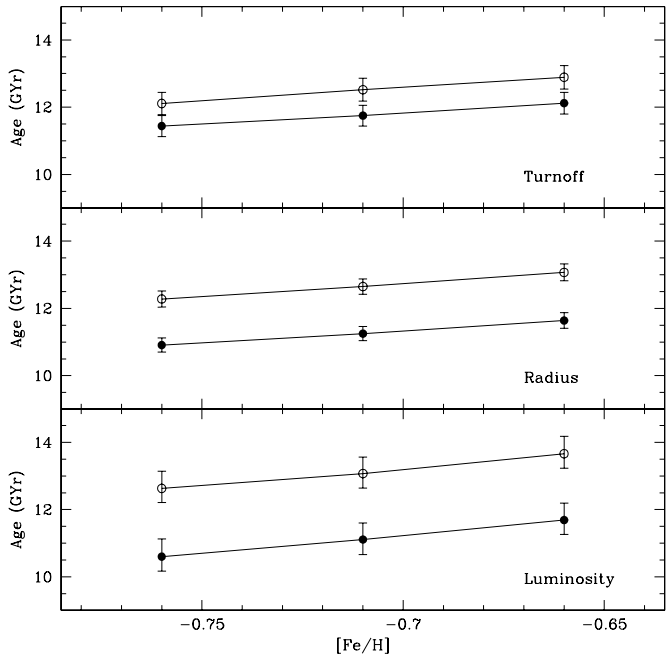

Figure 12. Age as a function of [Fe/H] for Dartmouth (filled symbols) and Yonsei–Yale (open symbols) models. Ages are determined from mass–luminosity relations (bottom panel), mass–radius relations (middle panel), and turnoff mass–age relations (upper panel).

6.2. Sensitivity to α-Element Enhancement

We have estimated the effect of differing α-element enhancement by measuring the ages of the components of V69 from Dartmouth and Yonsei–Yale isochrones calculated to have differing α-enhancement in the range 0.2–0.4 at a fixed [Fe/H] = −0.71. The results are shown in Figure 13, where we plot the weighted average of the ages measured for the primary and secondary components against model [α/Fe]. As we found for the sensitivity to adopted model [Fe/H], the slopes (in terms of Δ Gyr per 0.1 dex) are similar for the two model sets. The individual values and the averages are listed in Table 10.

6.3. Helium Abundance and Heavy Element Diffusion

At the adopted [Fe/H], the models span a modest but important range in helium abundance (Y), from $Y = 0.243$ for the Victoria–Regina models to 0.2555 for the Dartmouth models. The age estimates from mass–radius, mass–luminosity, and turnoff mass–age relations for all five model sets are plotted in the upper panel of Figure 14. An obvious trend in age with

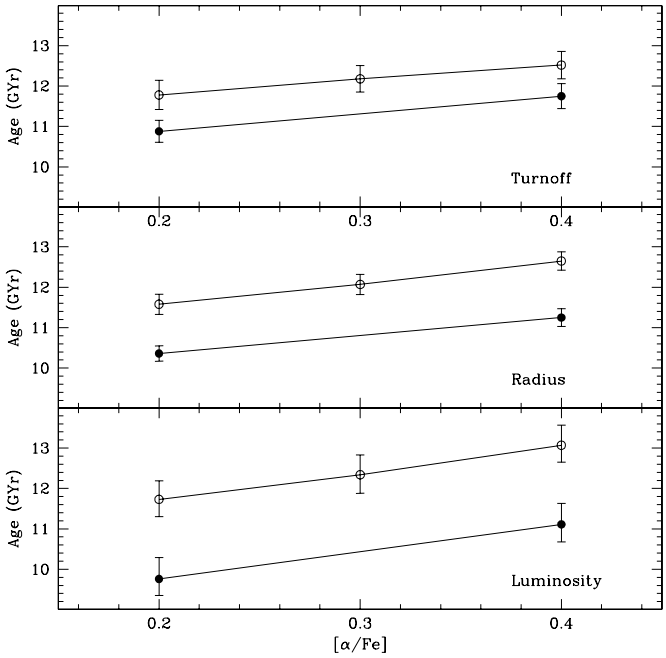

Figure 13. Age as a function of α-element enhancement for Dartmouth (filled symbols) and Yonsei–Yale (open symbols) models. Ages are determined from mass–luminosity relations (bottom panel), mass–radius relations (middle panel), and turnoff mass–age relations (upper panel).

Y can be seen in Figure 14 as expected. In order to further explore the dependence of age on Y, stellar evolution tracks were computed by one of us (Dotter) using the code described by Dotter et al. (2007) for [Fe/H] = −0.71 and [α/Fe] = +0.4 at Y = 0.24, 0.255, 0.27, 0.285, and 0.30 for the measured masses and $\pm 1\sigma$ uncertainties of the primary and secondary components of V69 (see Table 6). Ages were read from the tracks at the measured luminosities and radii of the components and plotted as open symbols in Figure 14 for all but the $Y = 0.30$ case. The plotted track-based ages are a weighted average of the ages of the primary and secondary components. These ages are listed in Table 11. The variation in measured ages with helium abundance for these tracks closely follows that seen for the five sets of model isochrones.

Some of the scatter seen in the upper panel of Figure 14 comes from two sources. First, the Victoria–Regina models are calculated for [α/Fe] = +0.3, while the other four model sets use +0.4. To account for this we adjusted the Victoria–Regina models by +0.49 Gyr and +0.67 Gyr for ages determined from the mass–luminosity and mass–radius relations, respectively (see Figure 13 and Table 10). Second, the Dartmouth and Yonsei–Yale models include the effects of helium and heavy element diffusion and gravitational settling while the Padova, Teramo, and Victoria–Regina models do not.[9] As a general rule, diffusion will lower the ages determined from models (Salaris et al. 2000; Chaboyer et al. 2001). To estimate the importance of diffusion in the measured ages, evolutionary tracks were also calculated by Dotter for $Y = 0.255$ but without diffusion. Ages determined from these tracks are plotted in the upper panel of Figure 14. It might be expected that the effect of diffusion will

[9] In fact, the situation is more complicated than this because the Dartmouth models employ a treatment of diffusion that is inhibited in the outer 0.01 $M_\odot$ of the star (Chaboyer et al. 2001). The Teramo models employ diffusion in the calibration of their solar model but not in models used to generate their metal-poor models and thus their predicted ages are indirectly affected by diffusion.

Table 11
Ages in Gyr for the Components of V69 Derived from Dartmouth Tracks

Method	Component	$Y = 0.24$	$Y = 0.255$	$Y = 0.255$[a]	$Y = 0.27$	$Y = 0.285$
Luminosity	Primary	13.51+0.64/−0.66	11.77+0.56/−0.65	12.27+0.56/−0.65	10.20+0.52/−0.63	8.77+0.51/−0.62
	Secondary	13.71+0.76/−0.87	11.85+0.72/−0.86	12.40+0.76/−0.93	10.16+0.71/−0.90	8.60+0.74/−0.93
	Average	13.59+0.49/−0.53	11.80+0.44/−0.52	12.32+0.45/−0.53	10.19+0.42/−0.52	8.72+0.42/−0.52
Radius	Primary	12.97 ± 0.32	11.53 ± 0.28	12.32 ± 0.30	10.23 ± 0.25	9.10 ± 0.22
	Secondary	12.98 ± 0.45	11.48 ± 0.40	12.49 ± 0.43	10.13 ± 0.36	8.94 ± 0.32
	Average	12.97 ± 0.26	11.51 ± 0.23	12.38 ± 0.25	10.21 ± 0.21	9.05 ± 0.18

Notes. [a] Tracks calculated without the effects of diffusion.

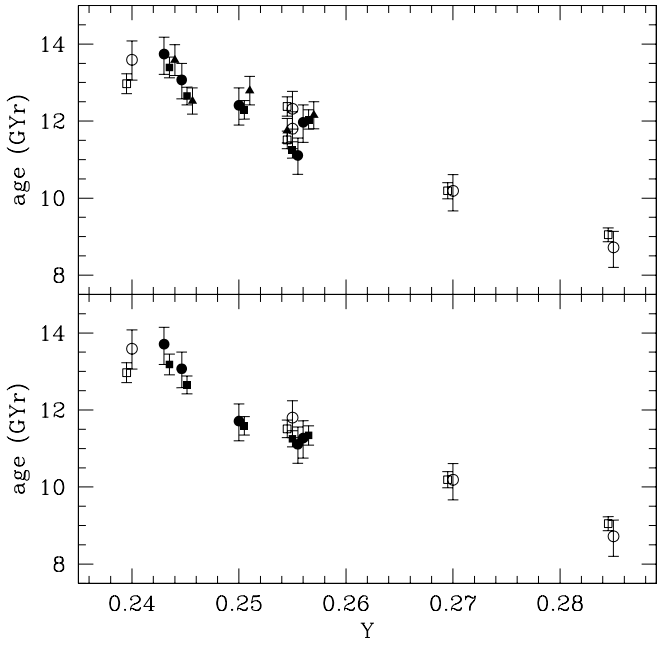

Figure 14. Age as a function of helium abundance as measured from Victoria–Regina, Yonsei–Yale, Padova, Dartmouth, and Teramo isochrones (solid symbols plotted left to right, upper panel). Ages are determined from mass–luminosity relations (circles), mass–radius relations (squares), and turnoff mass–age relations (triangles). Open symbols represent ages measured from Dartmouth tracks, see the text for details. Ages from two sets of Dartmouth tracks are plotted for $Y = 0.255$, models including helium and heavy element diffusion (lower ages) and models without diffusion (higher ages). The plotted points have been offset in helium abundance for clarity, the circles represent the correct helium abundance for any one model set. Bottom panel: ages corrected for the effects of diffusion (Victoria–Regina, Padova, and Teramo models). The Victoria–Regina ages have been additionally corrected to bring the α-element enhancement to +0.4.

depend on adopted helium abundance, and in the absence of a detailed comparison of diffusion in multiple model sets we adopt as a rough estimate a correction of −0.7 Gyr as measured from the Dartmouth tracks with and without diffusion. This correction was applied to the ages determined from the Padova, Teramo, and Victoria–Regina models. We note that evidence for diffusion is seen in the globular cluster NGC 6397 (Korn et al. 2007; Lind et al. 2008) based on a systematic variation of measured metal abundances from the turnoff through the giant branch. No such evidence was detected in 47 Tuc by Koch & McWilliam (2008), although the 47 Tuc sample only included one turnoff star.

The corrected ages are plotted in the bottom panel of Figure 14. There are two conclusions to be drawn from this figure. First, the measured ages continue to be tightly correlated with Y, and in particular, remaining residuals from this trend are not strongly related to [α/Fe], distribution of the α-element enhancements, or the mixing length. This correlation means that absolute ages of globular clusters based on individual stars in these clusters will be crucially dependent on an accurate measurement of the helium abundance of the cluster. This might seem impossible given the accuracy of various methods of determining cluster helium abundances (see, for example, Sandquist 2000). However, we note that for model sets with $Y \lesssim 0.25$, the ages measured from mass–luminosity and mass–radius relations differ systematically, with mass–luminosity relations predicting higher ages. This effect is reversed for ages measured from Dartmouth tracks for $Y = 0.285$. If the models are sufficiently accurate, it should then be possible to constrain both age and Y by requiring that the mass–luminosity and mass–radius ages be consistent.

We investigate the issue of helium abundance further in Figure 15 where we plot the measured radii and luminosities of the components of V69 together with Dartmouth tracks calculated for the masses of the primary and secondary for a range of values of the helium abundance. The measured values of the radii and luminosities of both the primary and secondary agree to within the uncertainties for $Y_p = 0.267^{+0.023}_{-0.029}$ and $Y_s = 0.271^{+0.024}_{-0.031}$ with an average value of $Y = 0.269^{+0.017}_{-0.021}$. This value can be compared with estimates of the helium abundance estimated from the population ratio $R = N_{\rm HB}/R_{\rm RGB}$ measured from ground-based photometry ($Y = 0.216^{+0.013}_{-0.015}$; Sandquist 2000) and *HST* photometry ($Y = 0.240 \pm 0.015$; Salaris et al. 2004). The agreement is reasonable given the uncertainties in the models used to calibrate the R method. There are at least two possible ways to improve upon our estimate. First, Figure 15 shows that our estimate is completely dominated by errors in the luminosities of the components of V69. Near-infrared eclipse photometry of V69 can be used to improve upon distance estimates, and hence luminosity estimates. Second, discovery of additional similar systems to V69 in 47 Tuc will help improve upon distance, age, and helium abundance measurements for this cluster.

Casagrande et al. (2007) derived bolometric luminosities and effective temperatures from multi-band photometry and the infrared flux method for a sample of 86 K-dwarfs. They compared these values to Padova stellar isochrones to estimate the He to metal enrichment ratio ($\Delta Y/\Delta Z$) in the solar neighborhood. Although their primary interest was to measure $\Delta Y/\Delta Z$, Casagrande et al. found that, in an absolute sense, the implied He content of the most metal-poor stars was as low as $Y \sim 0.1$—in marked disagreement with canonical values for the primordial He content (Salaris et al. 2004; Spergel et al. 2007). In contrast, we find no indication that current stellar evolution models are unable to reproduce the mass–radius relationship of V69.

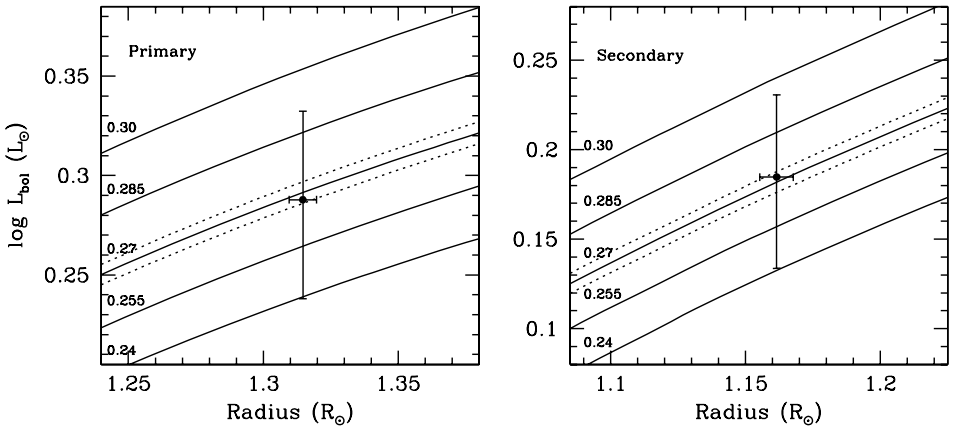

Figure 15. Dartmouth tracks calculated for the measured masses of the primary (left panel) and secondary (right panel). In each case the tracks are calculated for $Y = 0.24$ through $Y = 0.30$. The measured one sigma limits on mass are plotted as dotted lines for the $Y = 0.27$ tracks. The measured values of radius and luminosity for the components of V69 are both consistent with $Y = 0.27$ with a one sigma range of 0.03.

6.4. The Absolute Age of 47 Tuc

As mentioned above, a measurement of the absolute age of 47 Tuc will have random and systematic errors. Our best age estimates derived from the model isochrones have statistical errors of about 0.25 Gyr for mass–radius relations (see Table 9). Outside of remaining systematic errors arising from different model parameters, the main systematic errors arise from the empirical estimates for metallicity and α-element enhancement. We estimate the errors in both of these measurements to be 0.10 dex, and following the results in Table 10 we adopt a systematic error of 0.85 Gyr, the quadratic sum of the contributions from metallicity and α-element enhancement. This leads to an absolute age estimate of 11.25 ± 0.21(random) $\pm$ 0.85(systematic) Gyr from Dartmouth isochrones adopting $Y = 0.255$, [Fe/H] $= -0.71$, and [α/H] $= 0.4$. Note that the age estimate from the Teramo isochrones is very similar when a correction for diffusion has been applied (see Table 9 and Figure 14), as are the ages derived from mass–luminosity relations for both the Dartmouth and Teramo models. If we adopt a helium abundance of $Y = 0.27$ then the Dartmouth tracks indicate an age of $10.21 \pm 0.21 \pm 0.85$ Gyr.

This age estimate is consistent with other recent estimates of the age of 47 Tuc. For example, Gratton et al. (2003) find an age of 11.2 ± 1.1 by fitting model isochrones with no diffusion to the cluster color–magnitude diagram, and an age of 10.8 ± 1.1 Gyr for models including diffusion. Salaris & Weiss (2002) derive an age of 10.7 ± 1.0, also from isochrone fitting. Zoccali et al. (2001) obtain an age of 13 ± 2.5 Gyr by fitting the white-dwarf cooling sequence. Grundahl et al. (2002) concluded that the age of 47 Tuc is "slightly below 12 Gyr" based on analysis of Strömgren photometry and isochrone fitting. Our determination of the age of 47 Tuc based on observations of V69 has a small statistical error compared to that derived from isochrone fitting.

7. DISCUSSION AND SUMMARY

To the best of our knowledge, these measurements of the masses and radii of the components of V69 are the first such high accuracy (better than 1%) measurements to be made for Population II stars. The binary is a member of the globular cluster 47 Tuc and so the determination of its distance and age applies to the cluster as well. We obtained a distance modulus of $(m - M)_V = 13.35 \pm 0.08$. The main source of error in the distance estimate is the calibration-dependent estimate of effective temperatures which we used to derive the bolometric luminosities for the component stars.

A comparison of the measured masses, luminosities, and radii of the components to stellar evolution models suggests that the age of the system and hence the globular cluster 47 Tuc can be measured to a statistical accuracy of about 0.25 Gyr. However, it is important to understand the assumptions that go into any one model. In particular, the derived ages are very sensitive to the adopted helium abundance. We derive an age for 47 Tuc of $11.25 \pm 0.21 \pm 0.45$ Gyr for a helium abundance $Y = 0.255$ using Dartmouth model isochrones. All models give similar ages when the effects of helium abundance are taken into account.

Comparison of Dartmouth evolutionary tracks calculated for the measured masses of the primary and secondary indicate that the helium abundance can be measured to an accuracy of about 0.03 for each of the components. We estimate a helium abundance of $Y = 0.269^{+0.017}_{-0.021}$ for 47 Tuc. The measured masses, radii, and luminosities of the components of V69 are consistent with Dartmouth models assuming [Fe/H] $= -0.71$, [α/Fe] $= +0.4$, and $Y = 0.27$.

The radii of both stars are known with high accuracy, and it is therefore possible to obtain a more accurate and robust distance determination based on the surface brightness method (Barnes & Evans 1976; Lacy 1977; Thompson et al. 2001). The empirical calibration of surface brightness relations for dwarf and subgiant stars is improving (Di Benedetto 1998; Kervella et al. 2004; Buermann 2006), and it is reasonable to imagine that a distance accurate to a few percent can be measured with accurate radii and $(V - K)$ colors. We are in the process of collecting near-IR eclipse profile photometry of both V69 and V228 (Kaluzny et al. 2007b) in order to measure the distances to these two binary stars in this way. These data will improve the estimates of the bolometric luminosities of the components and lead to a more accurate measurement of the helium abundance and hence the absolute age of 47 Tuc.

Finally, we note that contributions to the errors in the radii are dominated by the photometric solution. Given the large inclination, the errors in the masses are completely dominated by the orbital solution. An identical doubling of the existing set of radial velocity observations leads to a 33% improvement in the mass estimates, and a subsequent improvement in the age estimates. The system is relatively bright, and the prospects are good that a substantial improvement in the measured masses can be achieved with further radial velocity observations.

J.K., W.P., and W.K. were supported by grant N203 379936 from the Ministry of Science and Higher Education, Poland.

Research of J.K. is also supported by the Foundation for Polish Science through the grant MISTRZ. I.B.T. is supported by NSF grant AST-0507325. Support from the Natural Sciences and Engineering Council of Canada to S.M.R. is acknowledged with gratitude. It is a pleasure to thank John Southworth and Willy Torres for sharing software with us. Jay Anderson kindly measured the proper motion of V69. I.B.T. acknowledges useful conversations with Chris Burns, Andy McWilliam, and George Preston. This research used the facilities of the Canadian Astronomy Data Centre operated by the National Research Council of Canada with the support of the Canadian Space Agency. We dedicate this series of papers to the memory of our colleague Bohdan Paczyński.

APPENDIX

In their catalog of 47 Tuc variables Weldrake et al. (2004) included a potentially interesting detached binary named V39. The object has an orbital period of 4.6 d and is located about 0.30 mag to the red of the cluster main sequence on the $V/V-I$ plane. We have obtained BV images of the V39 field using the du Pont telescope. These images show that V39 is a close visual pair of stars separated by 1.5 arcsec. The brighter component has $V \approx 18.1$ and $B-V \approx 0.99$ and is located on a $V/B-V$ CMD among the Small Magellanic Cloud (SMC) asymptotic giant branch stars. The fainter component has $V \approx 19.2$ and $B-V \approx 0.08$ and is a candidate SMC upper main-sequence star. Given the orbital period of V39 we propose that it is the fainter component of the blend which is the eclipsing binary.

REFERENCES

Alves-Brito, A., et al. 2005, A&A, 435, 657
Andersen, J. 1991, A&AR, 3, 91
Anderson, J., & King, I. R. 2003, AJ, 126, 772
Bahcall, J. N., Basu, S., Pinsonneault, M., & Serenelli, A. M. 2005, ApJ, 618, 1049
Barnes, T. G., & Evans, D. S. 1976, MNRAS, 174, 489
Bernstein, R., Shectman, S. A., Gunnels, S. M., Mochnacki, S., & Athey, A. E. 2003, Proc. SPIE, 4841, 1694
Blake, C. H., Torres, G., Bloom, J. S., & Gaudo, B. S. 2008, ApJ, 684, 635
Bono, G., et al. 2008, ApJ, 686, L87
Boyajian, T. B., et al. 2008, ApJ, 683, 2008
Brown, J. A., & Wallerstein, G. W. 1992, AJ, 104, 1818
Buermann, K. 2006, A&A, 460, 783
Carretta, E., Bragaglia, A., Gratton, R., & Lucatello, S. 2009, A&A, 505, 139
Carretta, E., & Gratton, R. 1997, A&AS, 121, 95
Casagrande, L., Flynn, C., Portinari, L., Girardi, L., & Jimenez, R. 2007, MNRAS, 382, 1516
Chaboyer, B., Fenton, W. H., Nelan, J. E., Patnaude, D. J., & Simon, F. E. 2001, ApJ, 562, 521
Clausen, J. V., Torres, G., Bruntt, H., Andersen, J. N., Stefanik, R. P., Latham, D. W., & Southworth, J. 2008, A&A, 487, 1095
Coelho, P., Barbuy, B., Meléndez, J., Schiavon, R. P., & Castilho, B. V. 2005, A&A, 443, 735
Di Benedetto, G. P. 1998, A&A, 339, 858
Dotter, A., Chaboyer, B., Jevremovic, D., Baron, E., Ferguson, J. W., Sarajedini, A., & Anderson, J. 2007, AJ, 134, 376
Etzel, P. B. 1981, in Photometric and Spectroscopic Binary Systems, ed. E. B. Carling & Z. Kopal (Dordrecht: Reidel), 111
Gebhardt, K., Pryor, C., Williams, T. B., & Hesser, J. E. 1995, AJ, 110, 1699
Gratton, R. G., Bragaglia, A., Carretta, E., Clementini, G., Desidera, S., Grundahl, F., & Lucatello, S. 2003, A&A, 408, 529
Grevesse, N., & Noel, A. 1993, in Origin and Evolution of the Elements, ed. N. Prantos, E. Vangioni-Flam, & M. Cassé (Cambridge: Cambridge Univ. Press), 15
Grevesse, N., & Sauval, A. J. 1998, Space Sci. Rev., 85, 161
Grundahl, F., Clausen, J. V., Hardis, S., & Frandsen, S. 2008, A&A, 492, 171
Grundahl, F., Stetson, P. B., & Anderson, M. I. 2002, A&A, 395, 481
Harris, W. E. 1996, AJ, 112, 1487
Kaluzny, J., Kubiak, M., Szymański, M., Udalski, A., Krzeminski, W., Mateo, M., & Stanek, K. Z. 1998, A&AS, 128, 19
Kaluzny, J., Pych, W., Rucinski, S., & Thompson, I. B. 2006, Acta Astron., 56, 237
Kaluzny, J., Rucinski, S. M., Thompson, I. B., Pych, W., & Krzeminski, W. 2007a, AJ, 133, 2457
Kaluzny, J., Thompson, I. B., Krzeminski, W., Olech, A., Pych, W., & Mochejska, B. 2002, in ASP Conf. Ser. 265, Omega Centauri, A Unique Window into Astrophysics, ed. F. can Leewen, J. D. Hughes, & G. Piotto (San Francisco, CA: ASP), 155
Kaluzny, J., Thompson, I. B., Rucinski, S. M., & Krzeminski, W. 2008, AJ, 136, 400
Kaluzny, J., Thompson, I. B., Rucinski, S. M., Pych, W., Stachowski, G., Krzeminski, W., & Burley, G. S. 2007b, AJ, 134, 541
Kelson, D. D. 2003, PASP, 115, 688
Kervella, P., Thévenin, F., Di Folco, E., & Ségransan, D. 2004, A&A, 426, 297
Kim, Y.-C., Demarque, P., Yi, S. K., & Alexander, D. R. 2002, ApJS, 143, 499
Koch, A., & McWilliam, A. 2008, AJ, 135, 1551
Korn, A. J., Grundahl, F., Richard, O., Mashonkina, L., Barklem, P. S., Collett, R., Gustafsson, B., & Piskunov, N. 2007, ApJ, 671, 402
Kraft, R. P., & Ivans, I. I. 2003, PASP, 115, 143
Lacy, C. H. S. 1977, ApJ, 213, 458
Lacy, C. H. S., Torres, G., & Claret, A. 2008, AJ, 135, 1757
Lacy, C. H. S., Torres, G., Claret, A., & Vaz, L. P. R. 2005, AJ, 130, 2838
Landolt, A. U. 1992, AJ, 104, 340
Lind, K., Korn, A. J., Barklem, P. S., & Grundahl, F. 2008, A&A, 490, 777
López-Morales, M. 2007, ApJ, 660, 732
López-Morales, M., Orosz, J. A., Shaw, J. S., Havelka, L., Arévalo, M. J., McIntyre, T., & Lázaro, 2006, arXiv:astro-ph/0610225
McLaughlin, D. E., Anderson, J., Meylan, G., Gebhardt, K., Pryor, C., Minniti, D., & Phinney, S. 2006, ApJS, 166, 249
Meibom, S., et al. 2009, AJ, 137, 5086
Neckel, H. 1986, A&A, 159, 175
Norris, J. E., & Da Costa, G. 1995, ApJ, 447, 680
Paczyński, B. 1997, in Space Telescope Science Institute Series, The Extragalactic Distance Scale, ed. M. Livio (Cambridge: Cambridge Univ. Press), 273
Percival, S. M., Salaris, M., van Vyk, F., & Kilkenny, D. 2002, ApJ, 573, 174
Pietrinferni, A., Cassisi, S., Salaris, M., & Castelli, F. 2006, ApJ, 642, 797
Popper, D. M. 1980, ARA&A, 18, 115
Popper, D. M., & Etzel, P. B. 1981, AJ, 86, 102
Prŝa, A., & Zwitter, T. 2005, ApJ, 628, 426
Ramirez, I., & Meléndez, J. 2005, ApJ, 626, 465
Salaris, M., Groenewegen, M. A. T., & Weiss, A. 2000, A&A, 355, 299
Salaris, M., Held, E. V., Ortolani, S., Gullieszik, M., & Momany, Y. 2007, A&A, 476, 243
Salaris, M., Riello, M., Cassisi, S., & Piotto, G. 2004, A&A, 420, 911
Salaris, M., & Weiss, A. 2002, A&A, 388, 492
Salasnich, B., Girardi, L., Weiss, A., & Chiosi, C. 2000, A&A, 361, 1023
Sandquist, E. L. 2000, MNRAS, 313, 571
Sarajdeni, A., et al. 2007, AJ, 133, 1658
Schlegel, D., Finkbeiner, D. P., & Davis, M. 1998, ApJ, 500, 525
Serenelli, A. M., Basu, S., Ferguson, J. W., & Asplund, M. 2009, ApJ, 705, L123
Southworth, J., Bruntt, H., & Buzasi, D. L. 2007, A&A, 467, 1215
Southworth, J., Maxted, P. F. L., & Smalley, B. 2004a, MNRAS, 351, 1277
Southworth, J., Zucker, S., Maxted, P. F. L., & Smalley, B. 2004b, MNRAS, 355, 986
Spergel, D. N., et al. 2007, ApJS, 170, 377
Stetson, P. B. 1987, PASP, 99, 191
Stetson, P. B. 1990, PASP, 102, 932
Stetson, P. B. 2000, PASP, 112, 925
Thompson, I. B., Kaluzny, J., Pych, W., Burley, G. S., Krzeminski, W., Paczyński, B., Persson, S. E., & Preston, G. W. 2001, AJ, 121, 3089
Torres, G., Boden, A. F., Latham, D. W., Pan, M., & Stefanik, R. P. 2002, AJ, 124, 1716
VandenBerg, D. A., Bergbusch, P. A., & Dowler, P. D. 2006, ApJS, 162, 375
VandenBerg, D. A., & Clem, J. L. 2003, AJ, 126, 778
van Hamme, W. 1993, AJ, 106, 2096
Weldrake, D. T. F., Sackett, P. D., Bridges, T. J., & Freeman, K. C. 2004, AJ, 128, 736
Wilson, R. E., & Devinney, E. J. 1971, ApJ, 166, 605
Wilson, R. E. 1979, ApJ, 234, 1054
Worthey, G., & Lee, H.-C. 2006, arXiv:astro-ph/0604590
Zoccali, M., et al. 2001, ApJ, 553, 733
Zucker, S., & Mazeh, T. 1994, ApJ, 420, 806